Research in Astronomy and Astrophysics, 25:075006 (7pp), 2025 July

https://doi.org/10.1088/1674-4527/adda7f
CSTR: 32081.14.RAA.adda7f

# Statistical Signatures of Gamma-Ray Burst 221009A in X-Ray Observations

Nabin Bhusal, Manjeet Kunwar, and Niraj Dhital
Central Department of Physics, Tribhuvan University, Kirtipur, Kathmandu 44618, Bagmati, Nepal; nabinbhusal25@gmail.com, manjeetkunwar04@gmail.com, nirajdhital@cdp.tu.edu.np
*Received 2025 March 26; revised 2025 May 11; accepted 2025 May 16; published 2025 June 10*

## Abstract

We perform a time-resolved statistical study of GRB 221009A's X-ray emission using Swift XRT Photon Counting and Windowed Timing data. After standard reduction (barycentric correction, pile-up, background subtraction via HEASOFT), we extracted light curves for each observational ID and for their aggregation. Count-rate histograms were fitted using various statistical distributions; fit quality was assessed by chi-squared and the Bayesian Information Criterion. The first observational segment is best described by a Gaussian distribution ($\chi^2 = 68.4$; BIC = 7651.2), and the second by a Poisson distribution ($\chi^2 = 33.5$; BIC = 4413.3). When all segments are combined, the lognormal model provides the superior fit ($\chi^2 = 541.9$; BIC = 34365.5), indicating that the full data set's count rates exhibit the skewness expected from a multiplicative process. These findings demonstrate that while individual time intervals conform to discrete or symmetric statistics, the collective emission profile across multiple observations is better captured by a lognormal distribution, consistent with complex, compounded variability in GRB afterglows.

*Key words:* Astronomical Databases – methods: statistical – Astronomical Instrumentation, Methods and Techniques

## 1. Introduction

GRB 221009A, observed on 2022 October 9, has been identified as one of the brightest gamma-ray bursts (GRBs) ever recorded (Dichiara et al. 2022). GRB 221009A is among the most well-documented GRBs to date, with observations spanning a wide range of wavelengths. It was detected by the Swift X-Ray Telescope (XRT) and has been extensively studied due to its extreme brightness and unique afterglow characteristics (Dainotti et al. 2022, O'Connor et al. 2023). The X-ray light curve (LC) of this event exhibits complex temporal behavior that requires detailed statistical analysis to uncover its underlying properties (Sakamoto et al. 2011, Margutti et al. 2013).

Swift was launched at 17:16 GMT on 2004 November 20 (Gehrels et al. 2009). According to NASA, Swift's primary goals are to "determine the origin of gamma-ray bursts, classify GRBs into categories, search for new types of bursts, and study how these bursts evolve and interact with their environment" (Gehrels et al. 2009). The XRT also enables imaging and spectral analysis of the GRB afterglow, offering valuable insights into the burst's characteristics (Sakamoto et al. 2008, Gehrels et al. 2009) The CCD operates at approximately −100°C to ensure low dark current and reduce proton irradiation effects (Breeveld et al. 2011, Pagani et al. 2007).

Statistical analysis plays a crucial role in understanding the temporal and spectral variability of GRBs (Guidorzi et al. 2009, Ukwatta et al. 2010). In this study, we analyzed the LC of GRB 221009A using three statistical distributions: Poisson, normal, and lognormal. The Poisson distribution is widely used to model count-based data, such as photon arrivals (Lyons 1986). The normal distribution is often employed to approximate symmetrical data, while the lognormal distribution is more suited for skewed distributions, which are common in astrophysical observations (Ajello et al. 2008, Basilakos et al. 2008).

GRB 221009A offers an unprecedented data set for X-ray time-series analysis (Götz et al. 2023). However, no published study has explicitly examined whether its X-ray counts follow a Poisson, Gaussian (normal) or lognormal distribution over different timescales or segments. Our analysis aims to determine which statistical model best describes the LC of GRB 221009A. By doing so, we provide insights into the emission processes by analyzing individual observation IDs for different starting observational IDs which detect counts. We assess the goodness of fit for each distribution using both the chi-square test and the Bayesian Information Criterion (BIC), aiming to determine the most suitable model for describing the observed data (Zhang et al. 2006). The results of this study can also contribute to broader discussions on GRB populations and their underlying physics which contribute to a better understanding of the statistical nature of GRB afterglow fluctuations and provide insights into the physical processes governing these high-energy phenomena.

The structure of the paper is as follows. Section 2 discusses data acquisition and pre-processing techniques. Section 3 presents the results and discussions followed by conclusions in Section 4.

## 2. Methods and Data Analysis

The analysis of GRB 221009A relied on software tools designed for theoretical interpretation and data extraction from the Neil Gehrels Swift Observatory, particularly in the X-ray energy band. The primary software package employed for this analysis was HEASOFT, a comprehensive suite of tools publicly accessible from the HEASARC website. This package includes essential utilities for handling Swift-specific data and provides the necessary tools for calibration, data cleaning, and analysis (HEASARC 2020a).

The software setup was carried out on a Linux-based system running Ubuntu OS v.20.04, chosen for its stability and compatibility with the HEASOFT package. The installation involved several key steps to ensure a seamless operational environment. First, the HEASOFT Version 6.30 source code was downloaded and installed, accompanied by the automatic installation of supporting tools such as FTools and the XANADU package, which includes XRONOS v.6.0 for timing analysis (HEASARC 2020a). Next, the Calibration Database (CALDB Version 1.02) was remotely set up. The calibration files were recovered from the Swift XRT. The CALDB repository was setup and integrated with the `xrtpipeline` tool to ensure high precision in data processing (HEASARC 2020b). Additionally, the DS9 (v.8.3) software was installed to facilitate the visualization and analysis of reduced data. The user-friendly interface of DS9 proved instrumental in efficiently analyzing the background and reduced data sets. Throughout the setup, official documentation guidance and supervisory input ensured a smooth and error-free process Heasarc (2020c).

Once the software environment was prepared, data for GRB 221009A were acquired from the Swift Observatory's XRT, which captures data in the energy range of 0.3–10 keV. The Swift XRT master catalog served as the primary source of all public Swift observations. The selection of observational data followed a systematic approach. Observations with exposure times greater than or equal to 900 s were prioritized to ensure adequate temporal coverage (Swift Observatory 2020). Positioning for GRB 221009A used was srcra = 288.3, srcdec = 19.7 (Swift Team 2022). Data files were downloaded, and any records containing errors were noted and excluded from further analysis. The downloaded data, Level 1 Swift/XRT data, were subjected to cleaning and calibration using the `xrtpipeline` tool from the HEASOFT package. Calibration files from the Swift/XRT CALDB repository ensured the integrity and accuracy of the preprocessed data. This extended temporal coverage allowed for detailed spectral and temporal analyses of the burst, significantly contributing to understanding its physical properties (Evans et al. 2009). We analyze data from Photon Counting (PC) mode and Windowed Timing (WT) mode by making a directory to save the cleaned output files, with accurate R.A. and decl. of the target source. We have generated the exposure map and corresponding error files. The data having higher count rates per second should be processed for pile-up (Arlt et al. 2013). After processing by `xrtpipeline`, the required files are obtained: `po_cl.evt`: The cleaned event file; `*.hk`: Housekeeping file; `ex.img`: Exposure map image. To perform barycenter correction on the cleaned data generated by the `xrtpipeline`, specific files from the `auxil` folder are copied to the corresponding output directories. The required files are: `pat.fits and sao.fits`. After copying the required files from the `auxil` folder to the output directory, barycentric correction was applied to adjust photon arrival times to the solar system's barycenter. This correction is essential for removing orbital effects, ensuring consistency across Swift XRT observations, and enabling precise timing analysis of transient and periodic phenomena (Capalbi et al. 2005).

For generating the necessary data products, we ran the `xrtproduct` tool from the HEASoft software package. This tool is specifically designed to process Swift XRT data, generating key outputs such as LCs and spectra. The processing steps involved filtering, binning, and cleaning the data to ensure accurate temporal analysis. The effective use of `xrtproduct` allowed us to extract reliable observational features for a comprehensive analysis (Capalbi et al. 2005). After performing barycenter correction and product, the next step is to use `Xselect`, which is a tool provided by the HEASARC software suite for analyzing data from space-based X-ray telescopes, like the Swift XRT. This tool is widely used for creating images, spectra, and LCs from the event data generated by these instruments (Capalbi et al. 2005, HEASARC 2020a). The primary objective of utilizing `Xselect` in our analysis is to extract data products with high-spatial and temporal resolution, including images and LCs from the cleaned event files, which are fundamental for detailed characterization and modeling of the X-ray source. The GBR 221009A, showing the $x$-pixels and $y$-pixels in the graph, can be defined by the picture, taken when the process of pile-up is done, as visualized in Figure 1.

### *2.1. Pile-up*

Pile-up occurs when multiple photons arrive within a detector's readout interval, leading to overlapping events that distort the recorded signal. This is common in high-flux sources, where the detector underestimates the true count rate. The region with maximum intensity is typically identified as the pile-up core, which is excluded or corrected to recover accurate information. By identifying this center, we can

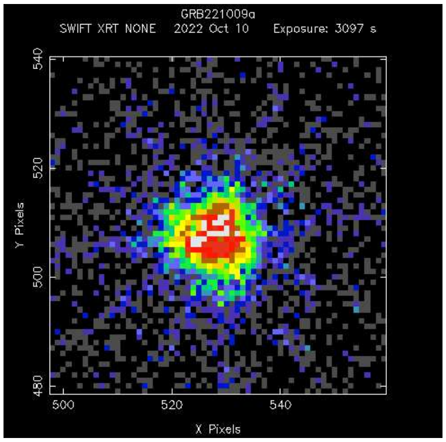


**Figure 1.** XRT PC mode image of GRB 221009A showing a central depression, a signature of photon pile-up. The observed count rate exceeds the critical threshold of 0.7 counts $s^{-1}$, signifying the condition for pile-up.

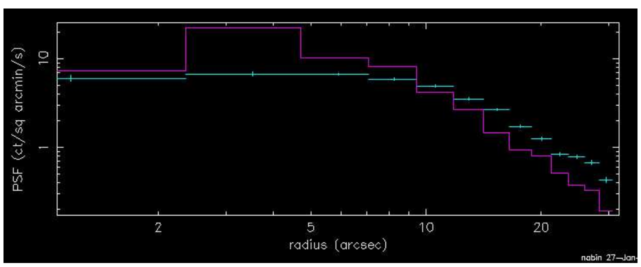


**Figure 2.** Radial profile of the PSF generated using `XIMAGE` tool in HEASOFT as a function of radius. The theoretical PSF (magenta) is compared to the observed PSF (cyan) for pile-up correction in the central region.

accurately model and mitigate the effects of pile-up in the analysis (Ballet 1999, Arlt et al. 2013). We consider the pile-up threshold to be more than 0.7 counts per second for PC mode and 100 counts for WT mode. If this condition is met, the data are then processed for pile-up correction. The data are subjected to the pile-up correction process by generating the point spread function (PSF) curve as shown in Figure 2.

### 2.2. *Lcmath*

To define the source region, we select a physical area corresponding to 20 pixels on the detector. This pixel size ensures accurate characterization of the source while minimizing the effects of pile-up. For the background analysis, we define an annular region with an inner radius of 30 pixels and an outer radius of 60 pixels. This annular region is chosen to isolate the background signal without including the source itself, allowing for a more accurate subtraction of the background from the total detected signal. LC analysis involves several computational steps to extract meaningful physical properties from observed data. In our study, we use the `lcmath` tool to perform background subtraction on LC files, ensuring accurate measurements of the source's flux (HEASARC 2025a). The process involves matching source and background LC files and applying mathematical operations to subtract the background contribution.

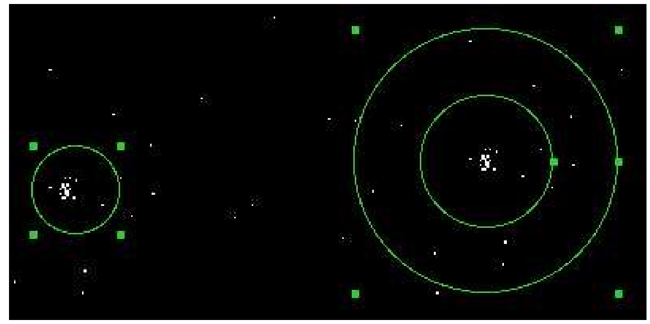

**Figure 3.** Image showing the result of background subtraction applied to the source region. This step is critical for isolating the target's emission and minimizing contamination in the derived LC.

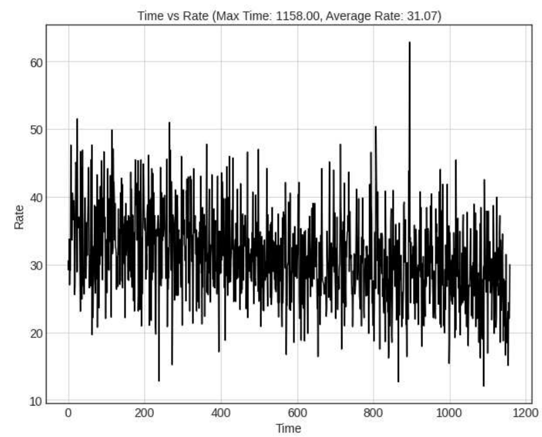


**Figure 4.** LC of GRB 221009A, in PC mode, for the first observation ID.

$$\mathrm{LC}_{\text{corrected}}(t) = \mathrm{LC}_{\text{source}}(t) - k \cdot \mathrm{LC}_{\text{background}}(t),$$

where $k$ is a scaling factor to account for differences in the extraction areas of the source and background regions. Background subtraction ensures that the final LC represents the intrinsic variability of the source (HEASARC 2025b). The corrected LC is then used for further analysis, including periodicity studies and modeling of flux variations. For the LC correction we make a 20 pc circle for the source and 30 and 60 annals for the background.

## 3. Results and Discussion

We performed a detailed statistical analysis of Swift XRT PC and WT mode data for GRB 221009A. We conducted a segment-wise statistical analysis. Each observational segment was evaluated against three statistical models-Poisson, normal (Gaussian), and lognormal distributions-based on goodness-of-

**Table 1**
Chi-squared Value Comparison Table

| Observation Set | Poisson $\chi^2$ | Normal $\chi^2$ | Lognormal $\chi^2$ | Best Fit |
|---|---|---|---|---|
| First Obs ID | 290.47 | 68.42 | 572.77 | Normal |
| Second Obs ID | 33.54 | 81.63 | 430.13 | Poisson |
| First and Second Obs IDs | $1.31 \times 10^7$ | 2513.47 | 2161.20 | Lognormal |
| 1st, 2nd and 3rd Obs Mix | $1.09 \times 10^{10}$ | 2593.60 | 2987.77 | Normal |
| All Obs with ID Mixing | $3.36 \times 10^{49}$ | $6.90 \times 10^{21}$ | 541.85 | Lognormal |

**Table 2**
Bayesian Information Criterion (BIC) Comparison Table

| Observation Set | Poisson BIC | Normal BIC | Lognormal BIC | Best Fit |
|---|---|---|---|---|
| First Obs ID | 7712.53 | 7651.21 | 7666.43 | Normal |
| Second Obs ID | 4413.34 | 4559.24 | 106428.45 | Poisson |
| First and Second Obs IDs | 22760.76 | 8330.78 | 5714.76 | Lognormal |
| 1st, 2nd and 3rd Obs Mix | 16455.74 | 7876.23 | 5629.01 | Lognormal |
| All Obs with ID Mixing | 347765.16 | 595007.66 | 34365.49 | Lognormal |

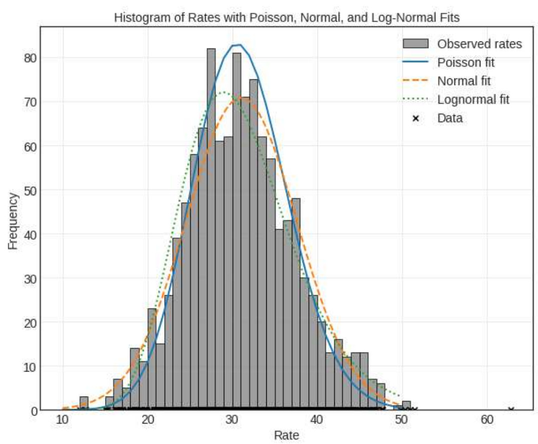


**Figure 5.** Histogram of the GRB 221009A, in PC mode, for first observation ID with fitting.

fit criteria: the chi-squared statistic and BIC (Press et al. 2007, Schwarz 1978).

Figures 4 and 5 illustrate the LC and corresponding rate histogram respectively for the first observational ID. Among the tested models, the normal distribution provides the best fit with $\chi^2 = 68.42$, as shown in Table 1. The Poisson model follows with $\chi^2 = 290.47$, while the lognormal distribution yields a poorer fit with $\chi^2 = 572.77$. The BIC values listed in Table 2 further support this outcome: the normal distribution exhibits the lowest BIC (7651.21), confirming its statistical preference for this segment.

Assuming a Poisson model for photon counts, we use the standard deviation $\sigma = \sqrt{\mu}$, where $\mu$ is the mean count rate. For the first ID with an average count of 31, this gives $dN = \sqrt{31} \approx 5.57$, leading to a signal-to-noise ratio (SNR) of 5.57, indicating a relatively bright detection (Wall & Jenkins 2012, Bevington & Robinson 2003, Gehrels 1986). This symmetry indicates that the variability in the X-ray flux is likely due to stochastic processes with a well-defined mean and standard deviation rather than extreme outliers. The Gaussian behavior implies symmetric flux variability likely governed by stochastic emission mechanisms, such as synchrotron radiation or thermal bremsstrahlung, rather than count-based discreteness typical of Poisson processes (Guidorzi et al. 2015).

The second observational ID, depicted in Figures 6 and 7, shows a decline in brightness with an SNR of 2.0. Here, the Poisson distribution provides the best fit ($\chi^2 = 33.54$), outperforming the normal ($\chi^2 = 81.63$) and lognormal ($\chi^2 = 430.13$) models. Corresponding BIC values confirm this (Poisson BIC = 4413.34 versus normal BIC = 4559.24), as noted in Table 2. These results suggest the emission process is dominantly discrete and stochastic, consistent with count-based photon arrival modeling rather than a smooth Gaussian variation (Cai et al. 2003). The poor lognormal fit suggests that the intensity variations do not strictly follow an exponential growth or decay pattern initially.

For this GRB, there is a zero count after these two observation, i.e., in the third observation ID. By mixing these two observation IDs, ignoring the time gap between them, we get the LC depicted in Figure 8, and the histogram of rates with Poisson, normal and lognormal fits displayed in Figure 9. We observe a shift in the statistical behavior. The lognormal

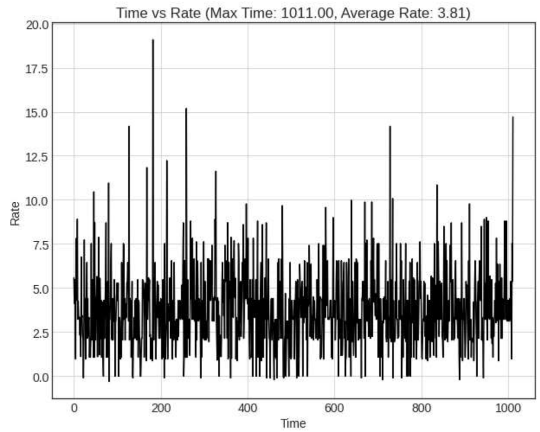


**Figure 6.** LC of the GRB 221009A, in PC mode, for the second observation ID.

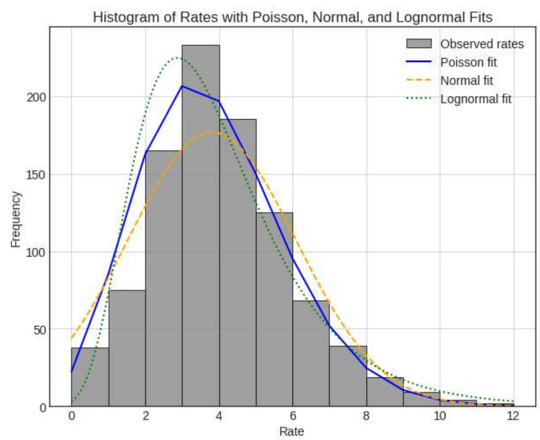


**Figure 7.** Histogram of the GRB 221009A, in PC mode, for the second observation ID with fitting.

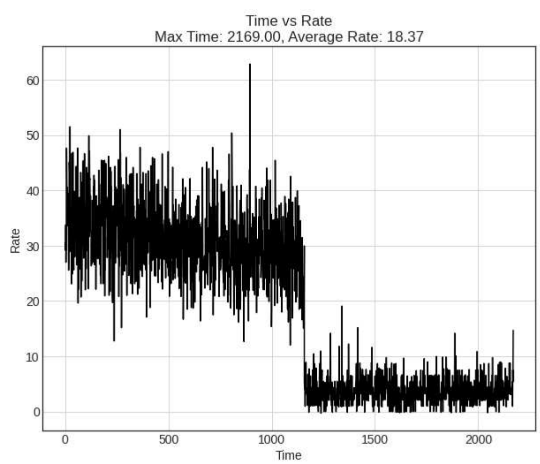


**Figure 8.** LC of the GRB 221009A, in PC mode, where the first two observation IDs are combined in a single plot.

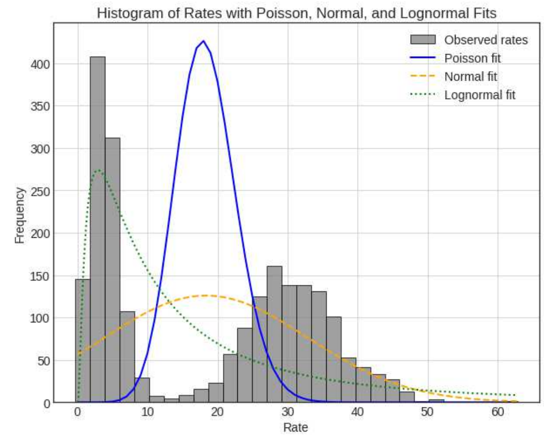


**Figure 9.** Histogram for the GRB 221009A, in PC mode, where first two observation IDs are combined in a single plot. In this plot, fitting is done for Poisson, normal and lognormal fits.

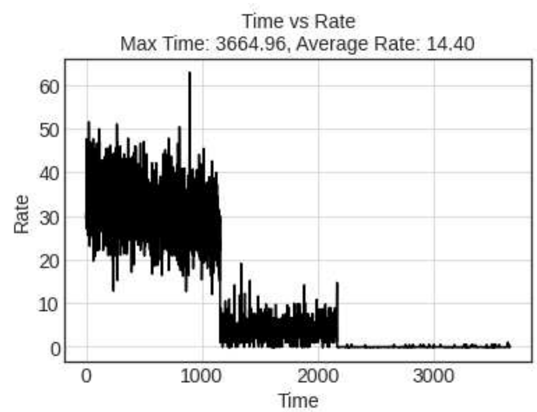


**Figure 10.** LC of the GRB 221009A, where the first three observation IDs are combined in a single plot.

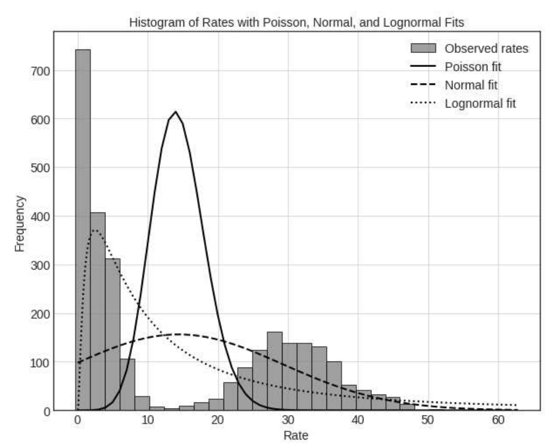


**Figure 11.** Histogram for the GRB 221009A, in PC mode, where the first three observation IDs are combined in a single plot. In this plot, fitting is done for Poisson, normal and lognormal fits.

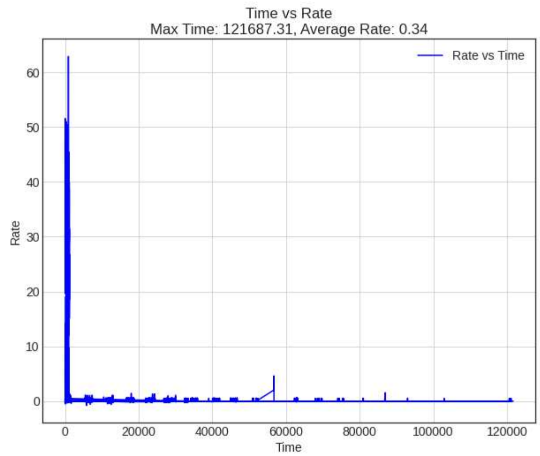


**Figure 12.** LC of the GRB 221009A, in PC mode, where all observation IDs are considered (up to 01126853084).

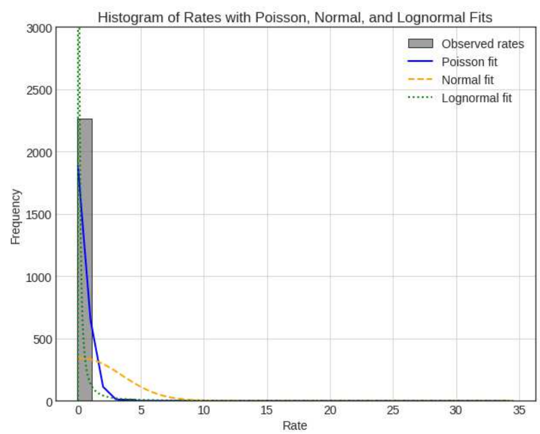


**Figure 13.** Histogram of rates with Poisson, normal and lognormal fits of the GRB 221009A, in PC mode, where all observation IDs are considered (up to 01126853084).

distribution emerges as the most appropriate fit with $\chi^2 = 2161.20$ and BIC = 5714.76, outperforming both the normal and Poisson models (see Tables 1 and 2). The substantial chi-squared value for the Poisson fit ($\chi^2 \approx 1.31 \times 10^7$) reflects an extreme outlier, indicating that the emission no longer follows a process with a constant rate (Guidorzi et al. 2024).

Extending the data set by incorporating a third observational ID (Figures 10 and 11), the trend continues. While the lognormal model still provides a competitive fit ($\chi^2 = 2987.77$), the normal distribution shows a marginally lower $\chi^2 = 2593.60$. However, the BIC values—normal BIC = 7876.23 versus lognormal BIC = 5629.01—strongly favor the lognormal distribution. The increasing skewness and variability in the composite data set favor a multiplicative stochastic process over an additive or discrete one.

Figures 12 and 13 show the LC and distribution respectively when all available observational IDs (up to 01126853084) are aggregated. The chi-squared values clearly illustrate that the Poisson ($\chi^2 \approx 3.36 \times 10^{49}$) and normal ($\chi^2 \approx 6.90 \times 10^{21}$) models are grossly incompatible with the data. In contrast, the lognormal distribution yields a significantly lower value of $\chi^2 = 541.85$, indicating superior fit quality. The corresponding BIC values (Poisson = 347765.16, normal = 595007.66, lognormal = 34365.49) confirm the statistical dominance of the lognormal model (Table 2).

The lognormal distribution captures the skewed nature of the XRT LC effectively, making it the most appropriate model for the full data set, as it aligns with the observed features of GRB 221009A. A lognormal emission profile implies a multiplicative underlying process, consistent with physical mechanisms such as synchrotron cooling or shock-driven variability (Zhang 2018, Zhang et al. 2006). This behavior is characteristic of many astrophysical transients, where energy dissipation occurs in intermittent bursts rather than smooth, additive changes (Li & Fenimore 1996, Sari et al. 1998).

## 4. Conclusion

This study provides a comprehensive statistical examination of the X-ray emission from GRB 221009A using Swift XRT data. Through chi-squared and BIC analyses, we find that the statistical nature of the emission evolves across time and observational coverage. In the earliest segments, the data are best described by Poisson or normal distributions, reflecting discrete photon events or symmetric stochastic processes respectively. However, when multiple observational IDs are aggregated, the lognormal distribution becomes statistically dominant, suggesting a multiplicative emission mechanism.

These findings are consistent with earlier works that reported extremely fast variability and complex prompt emission features in GRB 221009A. For instance, Lesage et al. (2023) showed that early-time variability was statistically indistinguishable from Poisson noise, aligning with our results for initial segments. Additionally, Zhang et al. (2023), Nousek et al. (2006) and Götz et al. (2023) interpreted the later prompt and early afterglow phases as involving structured jet dynamics and overlapping emission components, which could naturally lead to multiplicative variability and lognormal flux statistics over extended durations. Despite extensive temporal and spectral modeling in prior literature, no previous studies explicitly characterized the count-rate distribution or reported this linear to lognormal behavior.

Our results thus introduce a new dimension to GRB variability studies by demonstrating that, while individual pulses may follow Poisson-like or Gaussian behavior, the collective emission profile over time becomes distinctly lognormal. This supports the interpretation that GRB 221009A's emission is governed by internal shock processes or cascade-like energy dissipation, in which a series of independent fluctuations compound multiplicatively, consistent with theoretical expectations for turbulent jet environments (Kumar & Zhang 2015; Granot & Gill 2023; Rudolph et al. 2023).

Physically, this result aligns with the idea that GRB emission mechanisms may involve multiple overlapping processes. The initial prompt phase follows nearly normal statistical properties, possibly due to synchrotron or thermal bremsstrahlung radiation, where flux variations are symmetric around a mean value. However, as the GRB evolves, the emission process appears to be governed by multiplicative factors, such as turbulence-driven variations, jet interactions, or stochastic energy dissipation processes, leading to a lognormal distribution. The poor fit of the Poisson distribution for longer timescales suggests that GRB variability is not purely a count-based random process but involves complex temporal evolution.

## ORCID iDs

Nabin Bhusal https://orcid.org/0009-0002-1596-3638
Manjeet Kunwar https://orcid.org/0009-0000-7868-4199

## References

Ajello, M., Greiner, J., Sato, G., et al. 2008, ApJ, 689, 666
Arlt, J., Kliem, G., & Schmitt, M. 2013, RScI, 84, 103101
Ballet, J. 1999, A&AS, 135, 371
Basilakos, S., Plionis, M., & Georgantopoulos, I. 2008, MNRAS, 390, 190
Bevington, P. R., & Robinson, D. K. 2003, Data Reduction and Error Analysis for the Physical Sciences (3rd ed.; New York: McGraw-Hill)
Breeveld, A. A., Landsman, W., Holland, S. T., et al. 2011, in Proc. ASP Conf. Ser. 442, 23
Cai, C., Zhang, B., Li, Y., et al. 2003, MNRAS, 518, 2005
Capalbi, M., Perri, M., Saija, B., et al. 2005, The Swift XRT Data Reduction Guide, Version 1, 28 https://heasarc.gsfc.nasa.gov/docs/swift/analysis/xrt_swguide_v1_2.pdf
Dainotti, M. G., Levine, D., Fraija, N., et al. 2022, MNRAS, 518, 2201
Dichiara, S., Gropp, J. D., Kennea, J. A., et al. 2022, Brightest Gamma-ray Burst GRB 221009A: Observations and Implications, arXiv:2210.09000
Evans, P. A., Beardmore, A. P., Page, K. L., et al. 2009, MNRAS, 397, 1177
Gehrels, N. 1986, ApJ, 303, 336
Gehrels, N., Ramirez-Ruiz, E., & Fox, D. B. 2009, ARA&A, 47, 567
Götz, D., Mereghetti, S., Gros, A., et al. 2023, A&A, 677, L3
Granot, J., & Gill, R. 2023, MNRAS, 521, 1125
Guidorzi, C., Dichiara, S., & Frontera, F. 2015, ApJ, 801, 57
Guidorzi, C., Dichiara, S., Frontera, F., & Ruffini, R. 2024, Long Gamma-ray Burst Light Curves as the Result of a Common Stochastic Pulse-avalanche Process, arXiv:2403.18754
Guidorzi, C., Frontera, F., Montanari, E., et al. 2009, ApJ, 700, 1705
HEASARC 2020a, HEASOFT: The High Energy Astrophysics Software, https://HEASARC.gsfc.nasa.gov/docs/software/heasoft/
HEASARC 2020b, Calibration Database (CALDB) Version 1.02, https://heasarc.gsfc.nasa.gov/docs/heasarc/caldb/
HEASARC 2025a, LCMath Tool User Manual, https://heasarc.gsfc.nasa.gov/docs/xanadu/xronos/help/lcmath.html
HEASARC 2025b, ASCA Data Analysis: Background Subtraction, https://heasarc.gsfc.nasa.gov/docs/asca/abc/node10.html
Heasarc 2020c, DS9 (v.8.3): An Astronomical Data Visualization Software, http://ds9.si.edu
Kumar, P., & Zhang, B. 2015, PhR, 561, 1
Lesage, S., Burns, E., Meegan, C., et al. 2023, ApJ, 951, 72
Li, H., & Fenimore, E. E. 1996, ApJL, 469, L115
Lyons, L. 1986, Statistics for Nuclear and Particle Physicists (Cambridge: Cambridge Univ. Press)
Margutti, R., Soderberg, A. M., Wieringa, M. H., et al. 2013, ApJ, 778, 18
Nousek, J. A., Kouveliotou, C., Grupe, D., et al. 2006, ApJ, 642, 389
O'Connor, B., Troja, E., Ryan, G., et al. 2023, ApJL, 945, L12
Pagani, C., Morris, D. C., Racusin, J. L., et al. 2007, A&A, 469, 379
Press, W. H., Teukolsky, S. A., Vetterling, W. T., & Flannery, B. P. 2007, Numerical Recipes: The Art of Scientific Computing (3rd ed.; Cambridge: Cambridge Univ. Press) Chapter 15
Rudolph, J., Dermer, C. D., Zhang, B., et al. 2023, MNRAS, 524, 2447
Sakamoto, T., Barthelmy, S. D., Baumgartner, W. H., et al. 2011, ApJ, 669, 1115
Sakamoto, T., Hullinger, D., Sato, G., et al. 2008, ApJS, 175, 179
Sari, R., Narayan, R., & Piran, T. 1998, ApJL, 497, L17
Schwarz, G. 1978, AnSta, 6, 461
Swift Observatory 2020, Swift-XRT Master Catalog, https://www.swift.ac.uk/analysis/xrt/
Swift Team 2022, GRB 221009A Position Data, https://www.swift.ac.uk/xrt_positions/
Ukwatta, T. N., Stamatikos, M., Dhuga, K. S., et al. 2010, ApJ, 711, 1073
Wall, J. V., & Jenkins, C. R. 2012, Practical Statistics for Astronomers (2nd ed.; Cambridge: Cambridge Univ. Press)
Zhang, B. 2018, ApJ, 827
Zhang, B., Fan, Y. Z., Dyks, J., et al. 2006, ApJ, 642, 354
Zhang, B., Zhao, X., Zhang, Q., et al. 2023, ApJL, 946, L21